European Journal of Medicinal Chemistry 46 (2011) 3486–3498

Contents lists available at ScienceDirect

European Journal of Medicinal Chemistry

journal homepage: http://www.elsevier.com/locate/ejmech

Original article

Block of the hERG channel by bupivacaine: Electrophysiological and modeling insights towards stereochemical optimization

Liliana Sintra Grilo [a,b], Pierre-Alain Carrupt [a], Hugues Abriel [b], Antoine Daina [a,*]

[a] School of Pharmaceutical Sciences, University of Geneva, University of Lausanne, Quai Ernest-Ansermet 30, 1211 Geneva 4, Switzerland
[b] Department of Clinical Research, University of Bern, Murtenstrasse 35, 3010 Bern, Switzerland

ARTICLE INFO

Article history:
Received 27 August 2010
Received in revised form
3 May 2011
Accepted 5 May 2011
Available online 12 May 2011

Keywords:
Bupivacaine
Cardiotoxicity
Electrophysiology
hERG channel
Molecular docking
Stereoselectivity

ABSTRACT

The hERG voltage-gated potassium channel mediates the cardiac I_{Kr} current, which is crucial for the duration of the cardiac action potential. Undesired block of the channel by certain drugs may prolong the QT interval and increase the risk of malignant ventricular arrhythmias. Although the molecular determinants of hERG block have been intensively studied, not much is known about its stereoselectivity. Levo-(S)-bupivacaine was the first drug reported to have a higher affinity to block hERG than its enantiomer. This study strives to understand the principles underlying the stereoselectivity of bupivacaine block with the help of mutagenesis analyses and molecular modeling simulations. Electrophysiological measurements of mutated hERG channels allowed for the identification of residues involved in bupivacaine binding and stereoselectivity. Docking and molecular mechanics simulations for both enantiomers of bupivacaine and terfenadine (a non-stereoselective blocker) were performed inside an open-state model of the hERG channel. The predicted binding modes enabled a clear depiction of ligand–protein interactions. Estimated binding affinities for both enantiomers were consistent with electrophysiological measurements. A similar computational procedure was applied to bupivacaine enantiomers towards two mutated hERG channels (Tyr652Ala and Phe656Ala). This study confirmed, at the molecular level, that bupivacaine stereoselectively binds the hERG channel. These results help to lay the foundation for structural guidelines to optimize the cardiotoxic profile of drug candidates *in silico*.

1. Introduction

The human *Ether à-go-go* Related Gene channel (hERG) plays a central role in the repolarization phase of the cardiomyocyte action potential (AP), where it is responsible for the rapid component of the delayed rectifier potassium current (I_{Kr}), which determines AP duration [1]. hERG is a voltage-gated potassium channel (K_v) that consists of four identical α-subunits (Fig. 1A) encoded by the *KCNH2* gene. Many loss-of-function mutations in the *KCNH2* gene (see www.fsm.it/cardmoc) are responsible for causing *congenital Long QT Syndrome* (cLQTS), a genetic disorder characterized by a prolonged QT interval on the ECG due to reduced repolarizing currents [2]. Lengthening of the QT interval is linked to potentially lethal ventricular arrhythmias named *Torsades de Pointes* [3].

Numerous structurally diverse drugs, such as antifungal ketoconazole [4], antipsychotic chlorpromazine [5] and prokinetic cisapride [6], may unintentionally block the hERG channel, leading to the *drug-induced Long QT Syndrome* (diLQTS) [7]. This rare, yet serious adverse effect, led to the withdrawal of several drugs from the market, and raised the awareness of hERG toxicity in the health and pharmaceutical fields. Regulatory authorities published recommendations on a set of nonclinical as well as clinical investigations for hERG-liability [8]. According to Raschi et al. [9] and Shah [8], estimates are that about 60–70% of all new chemical entities may block the hERG channels *in vitro* and be abandoned from further development; this severely limits the introduction of new drugs into the pipeline for many therapeutic targets. Concomitantly, research involving the hERG channel and the block of potassium channel determinants dramatically increased. However, no solved crystal structure of hERG has been made

Abbreviations: AP, action potential; cLQTS, congenital long QT syndrome; diLQTS, drug-induced long QT syndrome; ECG, electrocardiogram; ES, extracellular solution; GB/SA, modified generalized born/surface area model; HEK293, human embryonic kidney 293 cells; hERG, human *ether-à-gogo* related gene; IC_{50}, half-maximal inhibitory concentration; I_{hERG}, rapid component of the delayed; I_{Kr}, rapid component of the delayed rectifier potassium current; K_v channels, voltage-gated potassium channels; $MHBP_{do/ac}$, molecular hydrogen-bonding potentials for donor and acceptor capacity; rmsd, root mean square deviation; WT, wild-type.

* Corresponding author. Tel.: +41 22 3793365; fax: +41 22 3793360.
E-mail address: antoine.daina@unige.ch (A. Daina).

0223-5234/$ – see front matter © 2011 Elsevier Masson SAS. All rights reserved.
doi:10.1016/j.ejmech.2011.05.015

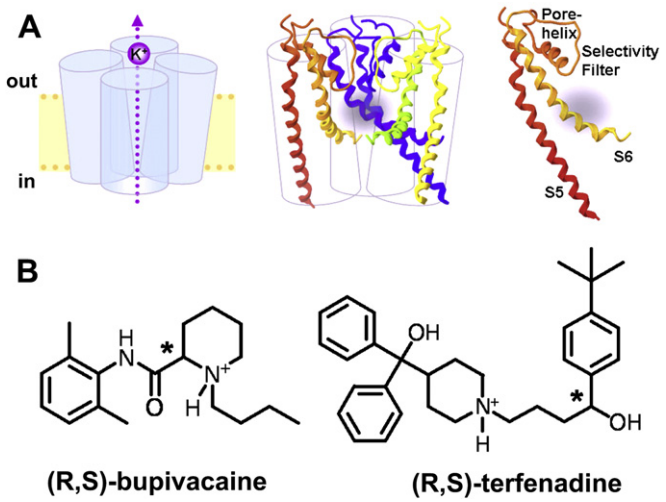

Fig. 1. Structure of hERG channel and blocking drugs. (A) Cartoon depicting the tetrameric structure of hERG voltage-gated potassium channel (*left*). For clarity, only three subunits are presented in order to show the pore–constituting unit (*middle*), which is formed by S5 and S6 transmembrane domains, the pore–helix and the selectivity filter (*right*). (B) Chemical structures of hERG blockers (R,S)-bupivacaine and (R,S)-terfenadine, protonated as at physiological pH and with the chiral center marked with an asterisk. Both structures encompass a piperidine ring N-substituted by an alkyl chain, and one aromatic ring within a similar distance from the basic nitrogen.

publicly available, at the time of writing this manuscript. Nevertheless, according to hydropathy plots and sequence similarity with other K_v channels, it may be proposed that each α-subunit is composed of six membrane-spanning helices (transmembrane domains S1-S6) and intracellular N- and C-termini. Enough information exists to reliably construct homology models of the pore-forming domain of hERG, consisting of transmembrane helix S5, the pore helix and selectivity filter (SF) and the S6 transmembrane domain (Fig. 1A). Most drugs are thought to block the channel inside its unusually large pore cavity [10]. Indeed, unlike other K_v channels, hERG lacks a Pro-X-Pro kink motif in the S6 helices that restricts inner cavity size [11]. The propensity of numerous and structurally diverse drugs to block the hERG channel is also due to the presence of aromatic residues (Tyr652 and Phe656) in the S6 domain that are known to interact with drugs. These amino acids are present in hERG and related *ether à-go-go* channels, but not in other K_v channels [12]. In addition to these two aromatic residues, other amino acids have been reported to affect drug block in mutagenesis studies (reviewed in [13]).

Although molecular determinants of hERG block have been intensively studied, not much is known about its stereoselectivity. Only a few studies directly address this issue in the literature [14–19], mainly regarding a widely used anesthetic, bupivacaine. Indeed, levo-(S)-bupivacaine (Fig. 1B) was the first drug reported to be more potent than its enantiomer (~2 fold) at blocking hERG currents *in vitro* [15–17]. In a recent review [20], however, we compiled examples of chiral drugs for which evidence exists that proarrhythmic cardiotoxicity may be caused by one enantiomer. Cited compounds include namely quinine/quinidine [21], methadone [14] and fluoxetine enantiomers (see Suppl. Fig. 1). Because of (R)-fluoxetine's shorter half-life, this enantiomer was thought beneficial in treatment of elderly individuals. However, clinical development of this enantiomer was stopped because of a statistically significant prolongation of the QT interval at high doses compared to the racemate (reviewed in [22]).

The work presented here focuses on bupivacaine and terfenadine, another drug with an asymmetric carbon atom (Fig. 1B). Terfenadine shares structural similarities with bupivacaine, and is also a potent hERG blocker [23,24]. Both structures have a piperidine ring N-substituted by an alkyl chain. Moreover, one of the terfenadine aromatic rings is at a comparable distance from the basic nitrogen compared to the *o,o*–dimethylphenyl of bupivacaine. Terfenadine was employed as an anti-histaminic drug until its adverse effects on hERG [25] and QT prolongation [26] led to its withdrawal from the market. In notable contrast to bupivacaine, putative stereoselective block of the hERG channel has never been reported for terfenadine.

We present here the stereoselective block of the hERG channel, analyzed with a double approach involving electrophysiological experiments and molecular modeling simulations. First, the inhibition of the hERG current by bupivacaine enantiomers was evaluated using the whole-cell patch clamp technique on cells expressing wild-type or selected mutant channels. In a second step, the block of hERG channels by bupivacaine was then studied using a fine-tuned structure-based methodology involving flexible docking, coupled with molecular mechanics treatments in order to rationalize the stereoselective binding at the molecular level. Altogether, we propose structural insights for stereochemical optimization of hERG-blocker drugs.

2. Results

2.1. Current block of wild-type and mutated hERG channels by bupivacaine enantiomers

Patch-clamp studies of bupivacaine perfusion on HEK293 cells expressing wild-type (WT) hERG channels show a clear stereoselective block of the measured K^+ current, with the levo-(S)-blocking more than the dextro-(R)-enantiomer (Fig. 2A). Inhibition values of the racemate are in-between those of the two enantiomers, and are significantly different from those of levo-(S)-bupivacaine. The dose-response data were mathematically described by Hill functions and the concentrations of half-maximal inhibition (IC_{50}) obtained for racemate and levo-(S)-isomer (32 ± 3 μM and 13 ± 1 μM, respectively) are in agreement with previous estimations [16], as presented in Table 1. As expected, dextro-(R)-bupivacaine has less affinity to block the hERG current (I_{hERG}), with an estimated IC_{50} of 84 ± 5 μM. Inhibition values of racemate and dextro-(R)-bupivacaine were not altered when currents were measured at 37 °C (data not shown).

In addition to the aromatic residues Tyr652 and Phe656 in the S6 helix, other amino acids important for high- and low-affinity drug binding to the hERG channel were identified by mutagenesis analyses. Based on published data reporting alanine scanning analyses of 20 drugs known to bind the K^+ channel [13], as well as comprehensive work on racemic bupivacaine block [27], we selected 7 amino acids individually mutated to alanine (Ala, A) in order to assess the stereoselective determinants of block. Three residues – Thr623 (T), Ser624 (S) and Val625 (V) – are located at the base of the selectivity filter, whereas the remaining four – Gly648 (G), Tyr652 (Y), Phe656 (F) and Val659 (V) – line the pore cavity on the S6 helix (inset, Fig. 3A). A preliminary screen of current block of the mutants was performed using 1 mM of bupivacaine. As previously noted by Siebrands and Friederich [27], some hERG mutants were low-expressing and required higher concentrations of extracellular K^+ to elicit larger inward tail currents. Several studies have confirmed that inhibition of hERG channels by bupivacaine is not affected by changes of external potassium levels when tail currents are measured at −120 mV [27,28]. Mutated hERG current traces (Fig. 3A) and properties are in agreement with formerly published studies [27,29,30].

According to the differences in enantiomeric block observed at a concentration of 1 mM, mutants of the K^+ channel can be

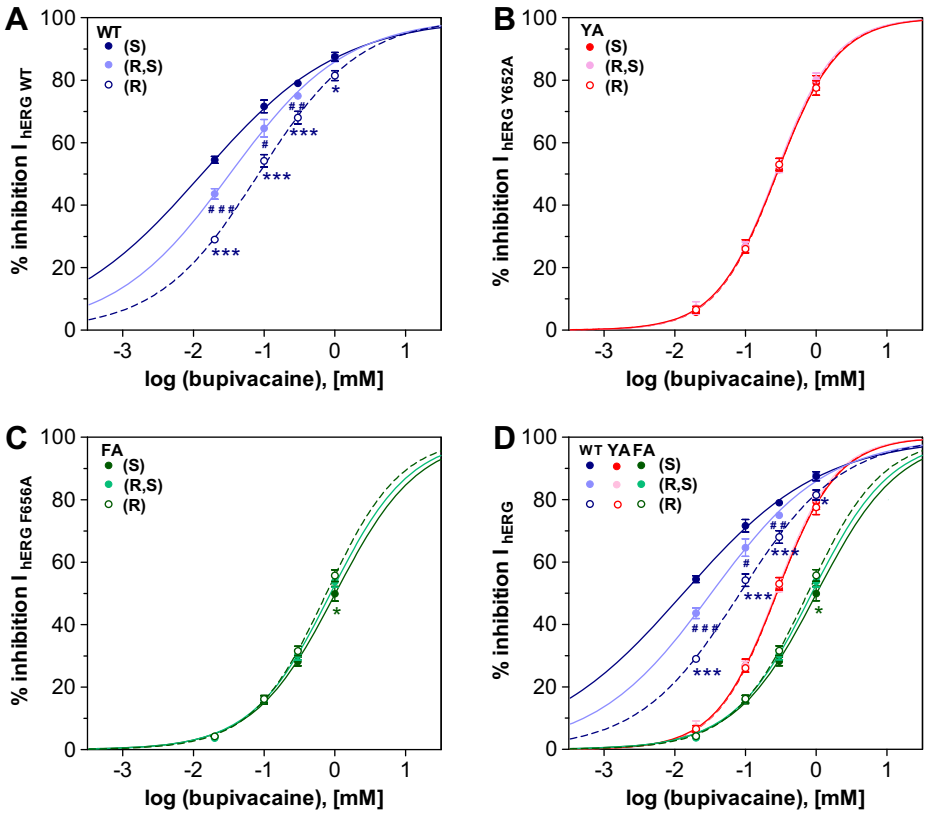

Fig. 2. Dose-response curves of inhibition of hERG current by bupivacaine forms. (A) Current inhibition (% inhibition of I_{hERG}) and drug concentration relationship for levo-(S)-, racemic (R,S)- and dextro-(R)-bupivacaine of hERG WT, (B) hERG-Y652A (YA) and (C) hERG-F656A (FA) channels. (D) Overlay of bupivacaine dose-inhibition curves show the marked stereoselectivity for hERG WT, the lack of difference for mutant Y652A (YA) and the reversal of stereoselectivity for mutant F656A (FA). Statistical differences compared with inhibition values of levo-(S)-bupivacaine are indicated ($P < 0.05$, */#; $P < 0.01$, ##; $P < 0.001$, ***/###).

classified as having: i) stereoselective block retained, ii) stereoselective block abolished or iii) stereoselective block reversed when compared to the WT channel (Fig. 3B). Channels mutated at the base of the selectivity filter behave like WT channels in presence of bupivacaine enantiomers, with significantly higher block produced by the (S)-enantiomer. hERG Y652A and V659A channels belong to the second group and have similar current block by the enantiomers. Finally, reversed stereoselectivity of bupivacaine block was seen for G648A and F656A mutants. Though local anesthetic concentration used was high, all mutated hERG channels had reduced current inhibition by bupivacaine compared to WT channels, with pronounced effects on F656A and V659A channels (Fig. 3A and B). The Y652A mutant was surprisingly not among the residues with the most current inhibition by bupivacaine. Dose-response curves of the mutants confirmed the loss of stereoselective block for Y652A (Fig. 2B), as well as the significantly higher block of F656A by dextro-(R)-bupivacaine (Fig. 2C). The IC_{50} of block for the racemate is increased ~10- and 30-fold compared to WT for mutants in position 652 and 656, respectively (Table 1). Hill slope (k) values for Y652A mutant are significantly higher than that of the WT channel (Table 1), and can explain why a minimal decrease in inhibition is observed at 1 mM, whereas an important difference is seen at lower concentrations (Fig. 2D). This emphasizes the importance of testing different drug concentrations in order to accurately assess mutagenesis effects.

2.2. Binding modes of terfenadine enantiomers in wild-type hERG

GOLD redocking of (S)-terfenadine in the chosen homology model was performed to calibrate the entire molecular modeling workflow prior to the docking of bupivacaine enantiomers. Parameters leading to the best overlap between the (S)-terfenadine solution and the native pose adopted in the model of Farid et al. [31] are described in the *Experimental section*. The block of hERG by terfenadine has not been previously reported to be stereoselective. Docking of (R)-terfenadine was concurrently performed in order to assess whether this can be interpreted at the molecular level. Selected docking solutions are presented in Suppl. Fig. 2A and show superimposed binding modes for both terfenadine enantiomers over the (S)-terfenadine, as found in Farid's homology model, with a remarkable overlap of all poses. Location of the chiral center

Table 1
Parameters derived from the Hill fit of the dose-response data of inhibition of hERG channels, WT and Y652A or F656A mutants.

		Levo-(S)-bupivacaine	Racemic (R,S)-bupivacaine	Dextro-(R)-bupivacaine
hERG WT	IC_{50} (μM) ± SEM	13 ± 1	32 ± 3	84 ± 5
		13 ± 1[a]	22 ± 2[a]	n.d.
	Hill slope ± SEM	0.44 ± 0.03	0.53 ± 0.04	0.61 ± 0.03
		0.85 ± 0.07[a]	0.91 ± 0.06[a]	n.d.
Y652A	IC_{50} (μM) ± SEM	278 ± 12	265 ± 13	276 ± 12
		83 ± 3[a]	95 ± 5[a]	n.d.
	Hill slope ± SEM	1.02 ± 0.05	1.03 ± 0.06	1.00 ± 0.05
		1.11 ± 0.05[a]	1.21 ± 0.07[a]	n.d.
F656A	IC_{50} (μM) ± SEM	1013 ± 84	866 ± 57	758 ± 42
		n.d.	n.d.	n.d.
	Hill slope ± SEM	0.75 ± 0.05	0.77 ± 0.04	0.83 ± 0.05
		n.d.	n.d.	n.d.

n.d. = not determined.
[a] Data obtained on Chinese Hamster Ovary (CHO) cells, from reference [16].

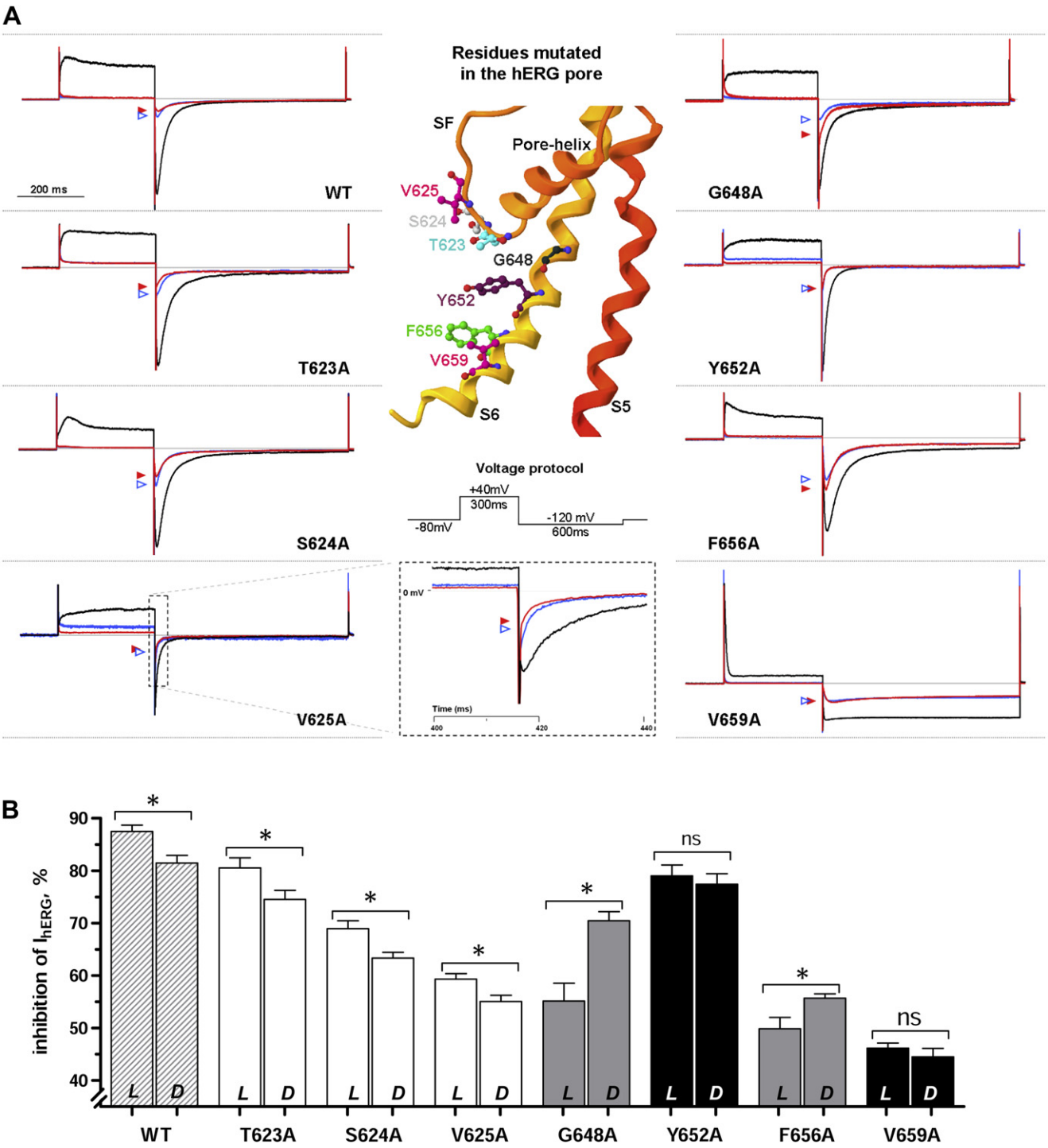

Fig. 3. Assessment of current block by perfusion of bupivacaine enantiomers at 1 mM in wild-type and mutated hERG channels. (A) Representative current traces through hERG WT and mutant channels evoked with the protocol in inset. Black traces represent the control current perfused with vehicle only. Dextro-(R)- and levo-(S)-bupivacaine blocks of current are respectively presented in blue and red traces, with peak amplitude noted by arrowheads of matching color. Location of the mutated residues in the S6 transmembrane helix and at the base of the SF is presented in the inset, with the color coding used in all figures. (B) Inhibition of I_{hERG} (% inhibition) for WT and mutant channels under perfusion of 1 mM of levo-(S)-bupivacaine (*L*) or dextro-(R)-bupivacaine (*D*) diluted in the ES. Bar fillings (except hERG WT, striated) with the following stereoselective-effect code: white, $L > D$; black, $L = D$, and gray, $L < D$. Two-sided Student's *t*–test was used for differences in current block by enantiomers ($P < 0.05$, *; ns, non significant) with $n = 5$–10 per enantiomer and mutant. The *y* axis is truncated (For interpretation of the references to colour in this figure legend, the reader is referred to the web version of this article.)

allows only minor conformational and positional changes between (R)- and (S)-enantiomers, primarily resulting in a flip of the hydroxyl group and rotation of the *tert*-butylphenyl end. Nevertheless, this aromatic group keeps its general location inside the hERG binding site, where it is involved in aromatic interactions with the residue Phe656. As expected by the constraint applied during docking runs (see *Experimental section*), the protonated nitrogen of both enantiomers closely interacts with Ser624 by donating a hydrogen to the side chain oxygen. The converging binding mode predicted for both enantiomers (Suppl. Fig. 2A) is consistent with the absence of stereoselectivity for the binding of terfenadine within the K^+ channel pore.

Force field post-processing (AMBER) of the docked ligands resulted in the final predicted binding modes presented in Suppl. Fig. 2B and C (solid stick representation). Molecular mechanics optimization of (S)-terfenadine inside the binding site only slightly affected the raw docking solutions. Detailed results are available in the supplementary material. In the optimized binding mode of the (R)-enantiomer, the diphenylmethanol substituent stays in its general location, but the piperidine and the *tert*-butylphenyl of (R)-terfenadine are displaced because the butanol linker finds favorable interactions lower in the binding site (Suppl. Fig. 3). Interestingly, only one hydrogen-bond remains (Suppl. Fig. 3A, tertiary alcohol and side chain of Ser649), and the interaction previously found in GOLD solutions between the basic nitrogen and Ser624 is lost. The loss of hydrogen-bonding would support higher binding affinity for the (R)-enantiomer of terfenadine, but the calculated free energy of binding for the (R)- and (S)-terfenadine was not significantly different with a Δ(ΔG) of −0.70 kcal/mol (Table 2). The loss of the (R)-enantiomer's strong polar interaction is likely counterbalanced by the hydrophobic interactions with one additional Phe656 residue (subunit III, Suppl. Fig. 3), as well as additional stabilizing π-stackings due to a better relative position of aromatic partners. Altogether, the overall computational results support the absence of stereoselective affinity of terfenadine enantiomers for the hERG channel.

2.3. Binding modes of bupivacaine enantiomers in wild-type hERG

After validation of our modeling strategy with terfenadine, the same methodology was used for the docking of dextro-(R)- and levo-(S)-bupivacaine towards the vestibule of the hERG channel. To ensure that results were not biased by the hydrogen-bond constraint, we simultaneously generated docking solutions without constraint. As this constraint was used to limit protein symmetry issues and facilitate the rmsd cluster analysis of solutions, convergence of the best docking solutions was sought out for both conditions. Binding modes obtained for bupivacaine enantiomers, in the presence or absence of constraint, were all located perpendicularly to the pore axis in the same region of the cavity. Most ligands in the study by Farid et al. [31] as well as our bupivacaine solutions were positioned just beneath the selectivity filter. Superimposition of the terfenadine and bupivacaine binding modes highlights some previously described pharmacophoric features [32–34]: the aromatic rings (*o,o*–dimethylphenyl group of bupivacaine and one phenyl ring of terfenadine) and the piperidine basic nitrogen show reasonably good overlap. The most striking difference between the binding modes of dextro-(R)- and levo-(S)-bupivacaine is the opposite orientation of the butyl chain (see Fig. 4). Docking solutions of bupivacaine enantiomers underwent force field treatment. This optimization procedure results in binding modes that were not significantly different from the original docking solutions (see detailed description in the supplementary material).

The final optimized binding modes of bupivacaine, originated from docking solutions without constraint, were analyzed considering pore residues that interact with the ligand, i.e. those with their atoms in a 5-Å shell. Good contacts between the ligand and near residues (see Experimental section) are displayed in Fig. 4, allowing for identification of amino acids involved in drug recognition. Residues Tyr652 and Phe656 are well-known molecular determinants of drug block, and this study highlights their contribution to bupivacaine binding. It is to note that Tyr652 of all four α-subunits are involved in good contacts with levo-(S)-bupivacaine, whereas only three participate in dextro-(R)-bupivacaine recognition. Residues of α–subunit I do not participate in dextro-(R)-bupivacaine binding, except for a slight contribution of Ser624 (Fig. 4A), whereas Thr623, Ser624, Ser649 and Tyr652 contribute to polar and steric contacts (with possibly minor hydrophobic contribution) with the (S)-enantiomer. Residues Ser624, Ser649 and Tyr652 (subunits II and III) are found in both binding modes. Additional steric and hydrophobic contributions of Thr623 (II) and Phe656 (III) are also observed in both binding modes (Fig. 4). Subunit IV also displays common residues for both enantiomers, most importantly Tyr652 that allows for parallel-displaced π-stacking interaction with the *o,o*–dimethylphenyl group. This α-subunit (IV) also has three residues at the base of the selectivity filter – Leu622, Thr623 and Ser624 – that contribute to both hydrophobic and polar interactions. Remarkably, Ser624 of subunit IV enables the formation of a hydrogen-bond with levo-(S)-bupivacaine, the side chain hydroxyl being the donor and the amide carbonyl acting as acceptor. Regarding bupivacaine (R)-enantiomer, this Ser624 is too far to form a hydrogen-bond.

In first approximation and in contrast to terfenadine, no obvious hydrogen-bond can be found between the piperidine nitrogen of both bupivacaine enantiomers and the hERG channel, even though this would have been favored by the applied docking constraint. A careful inspection of the optimized virtual complexes have not shown any possible polar interaction involving the R-enantiomer piperidine (Fig. 5A), whereas a weak hydrogen-bond of 3.3 Å can be considered between the acidic proton of the piperidine of the S-enantiomer and the oxygen of one Ser624 side chain (Fig. 5B). This surprisingly modest contribution of the basic group in molecular recognition can be explained by the drastically reduced hydrogen-donating capacity in its binding orientation as demonstrated by a Molecular Hydrogen-Bonding Potentials (MHBP) analysis. MHBP is a tridimensional procedure able to quantify both hydrogen accepting ($MHBP_{ac}$) and donating ($MHBP_{do}$) capacities in two modes, i.e. accounting or less for intramolecular non-bonded forces. The resulting difference between both modes assesses the effect of intramolecular interactions on the intermolecular hydrogen-bonding capacities for a given conformation [49,50].

The intramolecular effect of the bond conformation on the hydrogen donating potential is given in Fig. 5C *right panels* ($MHBP_{do}$ for S-bupivacaine; R-bupivacaine not shown). The lack of dots in the vicinity of the basic nitrogen in the *bottom right panel* illustrates the greatly reduced hydrogen donating potential compared to its moderate intrinsic capacity (as represented by yellow dots in the *upper right panel*). One can assume that the interacting amide oxygen internally "consumes" the basic nitrogen intermolecular hydrogen-bonding capacity. In contrast, terfenadine piperidine hydrogen-bonding potential is not decreased by any neighboring polar group and is consequently predicted as importantly participating in the molecular recognition of both enantiomers by the hERG channel.

Similarly, this conformational effect impacts partly the hydrogen accepting capacity of bupivacaine amide ($MHBP_{do}$ for

Table 2
Calculated Gibbs free energy of binding (ΔG, kcal/mol) within the AMBER 10 environment, including implicit solvation and surface terms for the different docked ligands within the hERG structure and estimated binding energy difference ($\Delta G_{(R)\text{-form}} - \Delta G_{(S)\text{-form}} = \Delta(\Delta G)$, kcal/mol).

	Ligand	ΔG, kcal/mol	Δ(ΔG), kcal/mol
hERG WT	(R)-terfenadine	−26.73	−0.70 **(S)=(R)**
	(S)-terfenadine	−26.03	
	dextro-(R)-bupivacaine	−17.14	+3.71 **(S)>(R)**
	levo-(S)-bupivacaine	−20.85	
Y652A	dextro-(R)-bupivacaine	−23.07	−0.76 **(S)=(R)**
	levo-(S)-bupivacaine	−22.31	
F656A	dextro-(R)-bupivacaine	−16.72	−0.15 **(S)=(R)**
	levo-(S)-bupivacaine	−16.57	

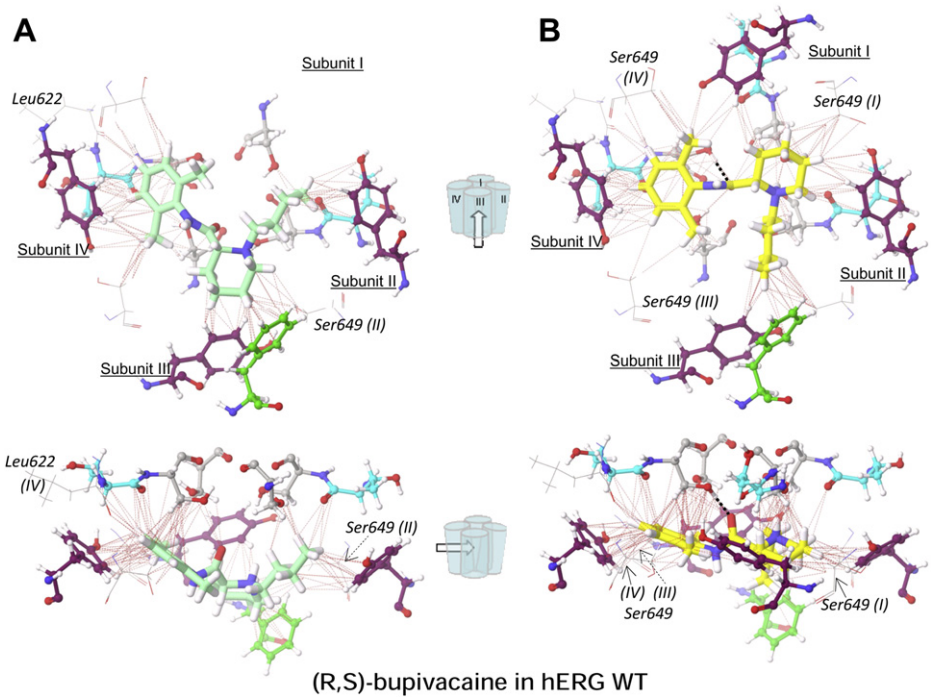

Fig. 4. Binding modes of bupivacaine enantiomers optimized by molecular mechanics in the hERG WT channel. (A) Dextro-(R)-bupivacaine (carbons in light green) or (B) levo-(S)-bupivacaine (carbons in yellow) are presented with hERG WT residues within a 5-Å shell, creating good contacts (red dashed lines) or hydrogen-bonds (black dotted lines) with the ligand. Both (A) and (B) are seen from two views as described by the scheme. Residues investigated in this study are highlighted with ball-and-stick representation and the following color-coding: Ser624, gray; Thr623, cyan; Tyr652, purple; Phe656, green, others are in wireframe with subunit number specified between brackets when necessary. Levo-(S)- and dextro-(R)-bupivacaine adopt different orientations of their butyl chain, thus keeping the amide carbonyl and protonated piperidine nitrogen facing the SF. However, only the levo-(S)-bupivacaine (closer to the SF) creates a hydrogen-bond with the side chain hydroxyl of one Ser624. In addition, the (S)-enantiomer interacts importantly with all four α-subunits (versus three for dextro-(R)-bupivacaine).

S-enantiomer in Fig. 5C *left panels*). One electronic lone pair on the oxygen interacts with the basic piperidine yielding a lack of dots on the right-hand side of the carbonyl in the *bottom left panel* compared to its full potential when intramolecular forces are not accounted for MHBP computation (orange and yellow dots in the *upper left panel*). Further detailed examination of the virtual complexes unveiled the role of the polar interactions between the carbonyl group and Ser624. In the case of dextro-(R)-bupivacaine, all four Ser624 residues create a crown-shaped hydrogen-bond network involving side chain hydroxyls and backbone carbonyls, with a weaker intermolecular interaction between Ser624 (subunit III) and the ligand carbonyl's second lone pair (Fig. 5A). Regarding levo-(S)-bupivacaine, a strong intermolecular hydrogen-bonding involving Ser624 (IV) and the second lone pair of the amide oxygen is clearly predicted as more favorable than the intra-protein hydrogen-bonding network (Fig. 5B).

The difference in the molecular recognition, the contribution of one additional subunit together with enhanced hydrogen-bonding network, is a central piece in the molecular modeling explanation for the higher current block experimentally described for levo-(S)-bupivacaine. Contrary to terfenadine, free energy of binding calculations predicted the (S)-enantiomer-hERG complex to be more stable than the complex with the (R)-enantiomer with a difference of 3.71 kcal/mol (Table 2). These results reveal a stereoselective binding of bupivacaine within the channel, with levo-(S)-bupicavaine showing higher affinity than the dextro-(R)-form.

2.4. Binding modes of bupivacaine enantiomers in hERG Y652A and F656A mutants

Our modeling strategy was applied likewise to the hERG mutants Y652A and F656A. For the F656A mutant, binding modes of bupivacaine enantiomers are located in the same cavity region as in the hERG WT pore. Global conformation of both enantiomers is comparable to that of the WT, particularly for the *o,o*—dimethylphenyl groups, since Tyr652 (subunit IV) still allows for parallel-displaced π-interaction with the aromatic moiety of bupivacaine (Fig. 6A). Unlike the docking solutions obtained in the WT channel, the α-subunits I, II and IV predominantly interact with both bupivacaine enantiomers, with only a slight contribution from subunit III. On three α-subunits (I, II and IV), serine residues (in position 624 and 649), Tyr652 and an adjacent Ala653, along with Thr623 on subunit IV, appear to be implicated in important steric contacts with both enantiomers of bupivacaine, involving to a certain extent hydrophobic contributions (Fig. 6A). For other amino acids implicated in molecular recognition, only slight differences are observed between the predicted binding modes for both enantiomers, such as minor hydrophobic contributions of Ser649 (III) and Ala653 (II) for (S)-bupivacaine binding versus Leu622 (IV) and Ser624 (II) for the dextro-(R)-formbupivacaine. As side chain volume of alanine is much reduced likened to the one of phenylalanine, it proves of interest to examine closer the steric changes. A cross-sectional view of the cavity solvent-accessible surface (Fig. 7) allows for assessment of shape variations; Phe to Ala mutation in position 656 widens the intracellular part of the vestibule, and subsequent rearrangement of adjacent amino acids rebuilds the upper vestibule into a cone. Bupivacaine enantiomers would, therefore, be sterically hindered from placement at the top of the cavity (Fig. 7C), as is seen with the WT channel (Fig. 7B). Due to favorable interactions with Tyr652 and the enlarged volume below this residue, the binding modes of bupivacaine enantiomers in the F656A channel are shifted downwards, but conserving the aromatic moiety as is found in the WT channel. Displacement of the amide carbonyl

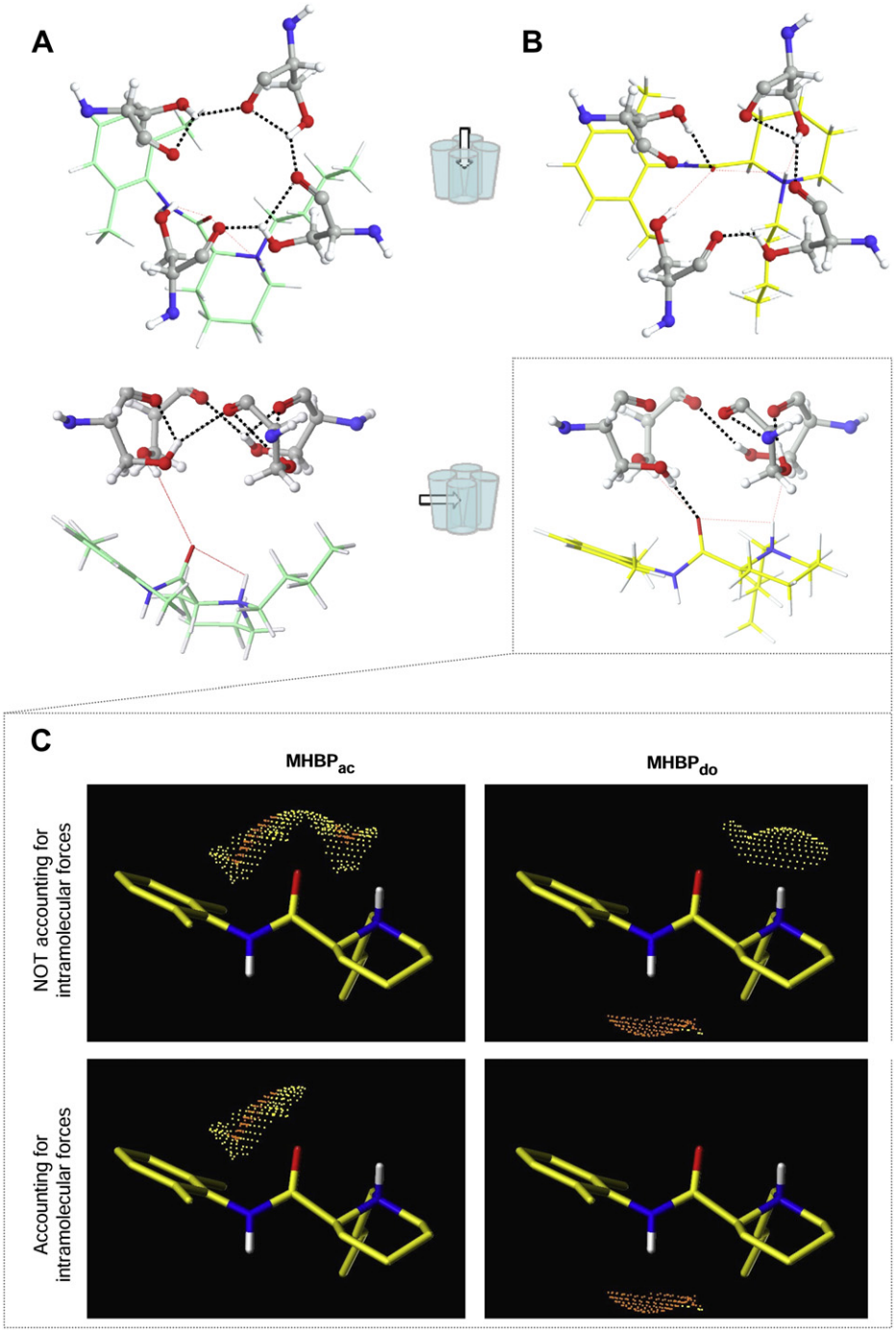

Fig. 5. Crown-shaped network of hydrogen-bonds involving Ser624 residues in the WT hERG channel, and hydrogen-bonding capacity by computing the MHBPs of levo-(S)-bupivacaine. (A) Optimized binding modes of dextro-(R)-bupivacaine (carbons in light green) and (B) levo-(S)-bupivacaine (carbons in yellow) observed from the viewpoint described by the central scheme (arrows). Residues Ser624 (ball-and-stick representation) from all four α-subunits present different intra- and intermolecular hydrogen-bonding networks (black dotted line) regarding (R)- and (S)-enantiomer poses. Closer location of the carbonyl of the amide in the levo-(S)-bupivacaine allows for the formation of a hydrogen-bond with one Ser624 side chain hydroxyl. Good contacts (red dashed lines) depict intra-molecular consumption of the capacity of the protonated piperidine nitrogen to create a hydrogen-bond with Ser624. In (A), a clear crown-shaped hydrogen-bonding network (distance cut-off: 2.5 Å) is seen involving side chain hydroxyls and backbone carbonyls of Ser624. (C) Representation of hydrogen-bonding capacity by computing the Molecular Hydrogen-Bonding Potentials (MHBPs) on a solvent accessible surface around the binding conformation of levo-(S)-bupivacaine. *Upper panels*: calculated acceptor (MHBP$_{ac}$) and donor (MHBP$_{do}$) potentials without taking intramolecular forces into account; *lower panels*: calculated acceptor (MHBP$_{ac}$) and donor (MHBP$_{do}$) potentials with intramolecular forces taken into account. For both donor and acceptor potentials, accounting for or neglecting the intramolecular forces explains the loss or decreased availability of both the carbonyl and the protonated amine for intermolecular interactions.

and protonated piperidine nitrogen lower in the binding site precludes any favorable polar interaction, as is seen inside the WT cavity with residues Ser624, which is consistent with the decreased affinity observed experimentally. The binding modes of bupivacaine enantiomers in the F656A cavity, as well as the free energy of binding calculations ($\Delta(\Delta G) = -0.15$ kcal/mol, Table 2), do not suggest stereoselectivity in favor of dextro-(R)-bupivacaine.

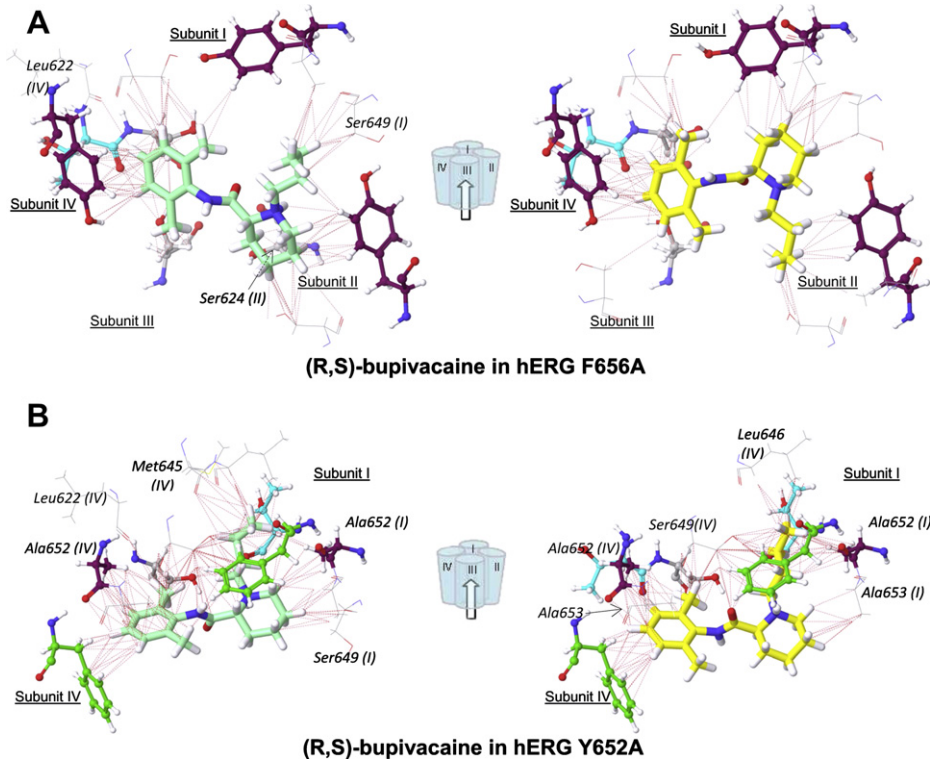

Fig. 6. Binding modes of bupivacaine enantiomers optimized by molecular mechanics in the hERG F656A and Y652A mutant channels. (A) Dextro-(R)-bupivacaine (carbons in light green) and levo-(S)-bupivacaine (carbons in yellow) inside the hERG F656A cavity, presented with good contacts (red dashed line). The poses obtained resemble the binding modes retrieved in the WT channel, except an important loss of residue participation in subunit I of hERG F656A. (B) Dextro-(R)-bupivacaine and levo-(S)-bupivacaine (same color-coding) inside the hERG Y652A cavity. Contrary to the results obtained with hERG WT and F656A channels, binding sites are lower and laterally shifted (contribution of two subunits only) in the Y652A cavity. In (A) and (B), viewpoints (arrows) are described by the central schemes. Residues investigated in this study are highlighted in a colored ball-and-stick representation (Ser624, gray; Thr623, cyan; Tyr652, purple; Phe656, green), while others are in wireframe and labeled (For interpretation of the references to colour in this figure legend, the reader is referred to the web version of this article.)

For the mutant of hERG-Y652A, docking solutions obtained with the hydrogen-bond constraint with Ser624 were clearly less homogenous than those without, indicating that its use yields an inappropriate bias for this mutated structure. Optimized final binding modes of bupivacaine, originated without constraint, reveal unexpected locations inside the cavity; bupivacaine molecules are lateral and not perpendicular to the pore axis, thus allowing for interactions with only two out of the four α-subunits (Fig. 6B). Variations in the solvent-accessible surface indicate that Tyr to Ala mutations extend the upper part of the binding site by opening side pockets. These pockets allow suitable accommodation of the N-butyl substituent of both enantiomers (Fig. 7D). Unlike other presented cases, both enantiomers have satisfactory overlap of all carbon atoms and do not present opposite orientations of the butyl chain. Analyses of binding modes indicate that phenylalanine residues in position 656 are crucial for stabilizing cation-π (subunit I) and T-shaped π-π (subunit IV) interactions with both enantiomers (Fig. 6B). Contrary to the hERG-F656A channel, mutated residues Ala652 are involved in hydrophobic interactions, mainly with the butyl chain. Some residues are involved in recognition of both enantiomers, including both hydrophobic and polar intermolecular forces, notably Thr623, Ala653 and the aforementioned Ala652 and Phe656 on subunit I, as well as Ser624, Leu646, Ser649 and Ala653, and Ala652 and Phe656 on subunit IV (Fig. 6B). Moreover, the residue Phe656 is implicated in the hydrophobic and aromatic stabilization of the *o,o*—dimethylphenyl ring. Differences observed laid in minor contributing residues, such as Ser649 (I), Leu622 and Met645 (IV) for the (R)-enantiomer, and Thr623 (IV) for the levo-(S)-bupivacaine. Similar docking poses and interacting residues let infer that there is no major difference in binding between the bupivacaine forms in the Y652A cavity. Considering the estimated free energy of binding (Table 2), (R)- and (S)-enantiomers have similar values of ΔG, being different by less than 1 kcal/mol and regarded as negligible. Altogether, the molecular modeling results support the absence of stereoselectivity of the bupivacaine enantiomers for the Y652A mutant of hERG channel.

3. Discussion

The raised concern about diLQTS impelled knowledge of structural determinants of hERG block; nevertheless, little is known about the stereoselective block of the delayed repolarizing potassium channel [14–18,20]. Chiral molecules with a stereoselective effect on the hERG channel could be highly informative with respect to the molecular requirements for drug binding and for safer enantiomeric drug development. We present here an electrophysiological and molecular investigation of the hERG channel's stereoselective block by bupivacaine enantiomers.

Through the use of the patch clamp technique on HEK293 cells expressing wild-type hERG channels, we confirmed the stereoselective block of hERG currents by levo-(S)-bupivacaine, as was originally described by Gonzalez and co-workers [15]. Our results show that levo-(S)-bupivacaine is ~7 times more potent at inhibiting I_{hERG} than its dextro-(R)-enantiomer. Levo-(S)-bupivacaine was commercialized because it was demonstrated to be a safer local anesthetic than its racemic mixture [35]. The purpose of this study is not to question the use of this enantiomer in anesthesiology, but rather to identify the molecular determinants that govern the stereoselective block of the hERG channel.

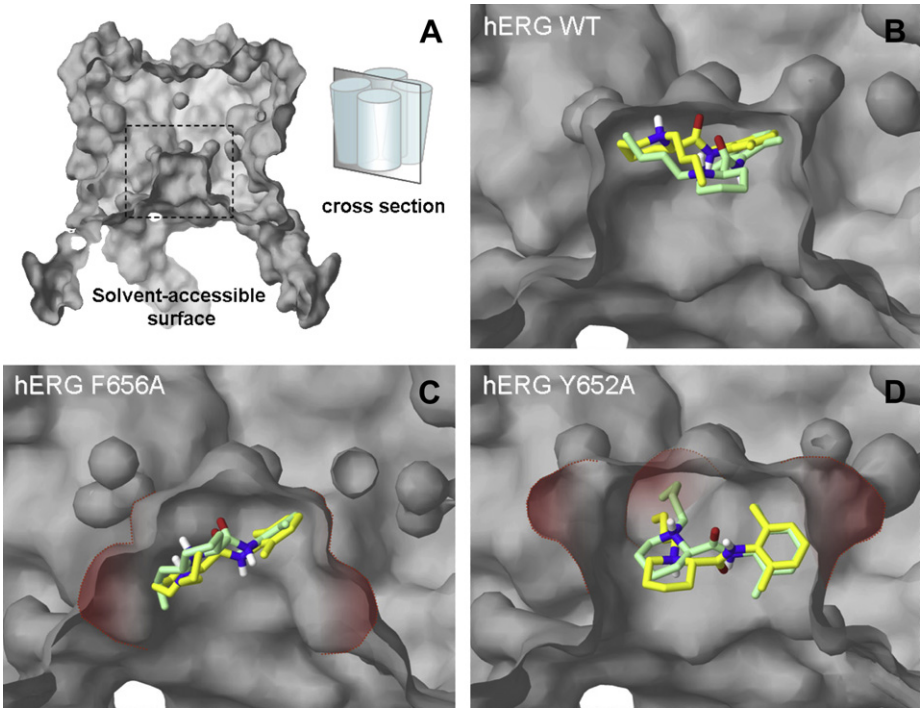

Fig. 7. Solvent accessible surface of hERG channel homology model with sagittal section through pore vestibule. (A) Cross section of the hERG channel solvent accessible surface using a probe of 1.40-Å radius. (B) Magnification of hERG WT binding site, (C) of mutant hERG F656A binding site with conic shape and (D) of mutant hERG Y652A binding site. In (B) to (D), optimized levo-(S)-bupivacaine (carbons in yellow) and dextro-(R)-bupivacaine (carbons in light green) binding modes are superimposed. Mutation of residues Tyr or Phe to Ala induces opening of new cavities (red shades) in the pore vestibule that alter the binding mode of ligands as compared to the WT hERG channel. (For interpretation of the references to colour in this figure legend, the reader is referred to the web version of this article.)

Prior to bupivacaine investigation, the computational strategy was validated by redocking the (S)-terfenadine enantiomer towards the described homology model. The difficulty of this particular docking case was due to the symmetrical nature of the ligands, as well as the tetrameric structure of the hERG channel, introducing rotational symmetry. The multiplication of different docking poses, representing identical binding modes due to the symmetry of the binding cavity, was overcome by adding a slight constraint favoring hydrogen-bond formation with one Ser624 residue. The predicted binding mode of the (S)-terfenadine is similar to that published by Farid et al. [31], though obtained by truly unrelated modeling techniques. Estimations of ΔG values provided supplementary evidence for the equal affinity of terfenadine enantiomers to the hERG binding site, which is consistent with the absence of reported stereoselective block.

Siebrands and Friederich [27] previously presented an electrophysiological study on the structural requirements of hERG block by racemic bupivacaine. Their conclusions were that all tested mutations – affecting residues Thr623, Ser624, Val625, Gly648, Tyr652 and Phe656 – reduced the inhibition of hERG currents by bupivacaine. We demonstrated that the valine residue in position 659 mutated to alanine (V659A) also importantly decreases the sensitivity to current block by bupivacaine. Based on these results, we measured the current inhibition of hERG channel mutants, which permitted their classification according to the relative potency of block by bupivacaine enantiomers.

The mutation of residues near the selectivity filter (positions 623, 624 and 625) retained the same stereoselectivity of bupivacaine block as the WT channel. Interestingly, Siebrands and Friederich [27] described a significant contribution of these three amino acids to the interaction with bupivacaine. Our predicted binding modes of levo-(S)-(S)- and dextro-(R)-bupivacaine within the WT channel vestibule show how Ser624 and Thr623 directly interact with the ligand through electrostatic contacts, but not Val625. The V625A mutation could indirectly affect bupivacaine binding through local changes of the shape and properties of the SF. The importance of the hydrophilic volume at the selectivity filter entrance has been previously highlighted in a study by Farid et al. [31], in which they stated that a "propeller-shaped" hydrophilic volume accepted basic groups of blockers to form electrostatic interactions with Ser624, instead of a generally accepted cation–π interaction with Tyr652. The importance of this serine residue for binding was confirmed in Kamiya et al. [36], where it was shown that the mutation S624A significantly decreased terfenadine block of hERG. With respect to the retained stereoselectivity, it appears that the polar residues at the base of the SF are necessary for binding but not determinant for enantiomeric recognition, meaning that the roots of stereoselective block reside in other amino acids.

Two mutated residues abolished enantiomer differences of I_{hERG} block – Tyr652 and Val659 – and two others led to the reversal of stereoselectivity of the current block – Gly648 and Phe656. Tyr652 and Phe656 are close enough to the bupivacaine ligands to directly interact, but residues in positions 648 and 659 are not within a 5 Å distance. Considering G658A, mutation of glycine to alanine should not drastically change the volume of the side chain. Importantly, Gly648 was long thought to be the glycine hinge that enables bending of the S6 and opening of the hERG channel [12,37] because it is located close to the Pro-X-Pro motif conserved in K_v channels [38]. This is a matter of debate as the detailed work by Hardman and colleagues [30] revealed that, conversely to what was expected, glycine residues are not required for flexibility, but rather for the tight packing of the S6 helix. Their results showed that substitution of Gly648 shifted the gating equilibrium to favor the open state. Siebrands and Friederich [27], however, reported that G648A was continuously opened. Taking together these findings, even a small change of side chain volume at position 648 might affect packing and

intra-helical interactions, and could explain the indirect involvement of this amino acid in drug binding. It is noteworthy that the nearby residue Ser649 appears important for electrostatic interactions with both terfenadine and bupivacaine enantiomers. Previous observations [31] suggested that aromatic side chains at positions 652 and 656 are highly sensitive to variation in the backbone conformation of Gly648 between their closed versus open model – the latter model serving as the basis for our target-based study. Conformational and gating changes might also account for the effect of V659A on bupivacaine enantiomer block. Mutation of this residue dramatically reduced the deactivation rate [10]. Consequent impairment in drug trapping [39] could explain the reduced sensitivity of this mutant to many drugs [13], including bupivacaine.

Finally, the aromatic residues Tyr652 and Phe656 were shown to be critical for both the affinity of binding and the stereoselectivity of block. Predicted binding modes of bupivacaine enantiomers highlighted the contribution of Tyr652 (subunit IV) to a highly favorable π–interaction with both (R)- and (S)-ligands. On subunit III, Phe656 appears to interact equally with both enantiomers through hydrophobic contacts. Discrepancy between interacting residues is seen in the number of α-subunits involved (four for levo-(S)- and only three for dextro-(R)-bupivacaine), of which the main stabilizing hydrophobic/aromatic good contacts involve tyrosines. The crucial role of Tyr652 and Phe656 aromatic residues in drug binding has long been attributed to formation of π–stacking interactions with aromatic rings, as well as cation–π interactions with the basic group of the ligand [29,40]. Farid et al. [31] and Zachariae et al. [41] assign the importance of these protruding amino acids to their concentric arrangement in the cavity allowing for multiple aromatic and/or hydrophobic interactions with various combinations of Tyr652 and Phe656 side chains. A striking observation considering all the bupivacaine enantiomer docking poses and refined virtual complexes is the systematic overlay of the *o,o*–dimethylphenyl group. This electron-rich aromatic appears to be very favorably stabilized by much electron-poorer rings, such as side chains of phenylalanine and especially tyrosine. This is likely an important pharmacophoric feature of hERG channel affinity. Moreover in our binding models, hydrogen-bond formation between the Ser624 hydroxyl and the carbonyl of the (S)-enantiomer emphasizes the binding affinity difference. It is worth to mention that the hydrophilic volume at the entrance of the SF, which favors polar interactions with the amide carbonyl and to a lesser extent with the basic nitrogen, obliges bupivacaine enantiomers to adopt poses with opposite orientation of the alkyl chain. Such a constraint of positioning is not seen for terfenadine due to the small size, flexibility and amphiprotic nature of hydroxyl substituent on the asymmetric carbon.

Molecular docking studies towards Y652A and F656A mutants proved to be insightful. Expected changes in side chain volume lead to the reshaping of the hERG binding site. In the case of the F656A mutation, bupivacaine enantiomers adopt a diagonal binding mode, though globally similar to those observed for the hERG WT since important aromatic interactions with tyrosine side chains are effective. Electrostatic interactions with Ser624 are no longer observed since the oblique positioning of enantiomers moves away the amide carbonyl of bupivacaine. Residues identified as creating good contacts with bupivacaine are noticeably the same for both enantiomers. This is consistent with the equivalent predicted free energy of binding, but not with the patch clamp results, which revealed a slight but significant reversal of stereoselectivity for the F656A channel. However, IC_{50} values of enantiomers presented only a ~1.25–fold difference and reside in the mM range. In other words, our molecular strategy fails in retrieving a tiny difference between two poor blockers of the hERG current, which, in addition, may not be clinically relevant.

Remarkably, binding modes of the bupivacaine ligands in the Y652A channel appear to be completely unlike that previously predicted in the WT and the F656A mutant. The major role of aromatic residues is disclosed by the retrieved binding modes. In the absence of Tyr652 residues, which are strong determinants of binding in the WT channel, the ligand finds other favorable interacting partners in the promiscuous hERG vestibule. Due to the reduction of side chain volume, new openings in the cavity allow for the accommodation of the butyl chain of (R)- and (S)-enantiomers, furthermore stabilized by hydrophobic interactions with the introduced Ala652. Phe656 appears to be an important feature for bupivacaine binding in Y652A cavity due to aromatic contributions (T-shaped and cation-π interactions). Altogether, the similar interacting residues in binding modes, the negligible differences in calculated free energies of binding and the comparable I_{hERG} block strongly support the abolishment of bupivacaine stereoselectivity in hERG Y652A. Extension of the binding site, coupled with lateral positioning of the ligands, leaves a large passage (~8–10 Å) between the intracellular side and the SF. Interestingly, Hill slope values are significantly higher for the inhibition of Y652A than WT and F656A hERG currents. This suggests that another molecular mechanism of block may be involved, such as the hypothetical accommodation of two molecules in the larger mutant cavity.

Another remarkable question raised by the positioning of the ligands in the cavities is the direct relationship between the affinity of binding and the potency of I_{hERG} block. Binding mode analyses in the WT hERG cavity show that the bupivacaine enantiomers are perpendicular to the pore axis, and that, along with important recognition forces with near SF residues, it transforms the molecule into a good "physical plug" which blocks the flow of K^+ ions. Moreover, bupivacaine molecules showed very favorable interactions in the Y652A cavity (ΔG), suggesting a high affinity of binding. At the level of IC_{50} of current block, values for the racemate are almost 10 times higher than that of the WT channel. As aforementioned, despite an important affinity of binding, the lateral positioning of the ligands in the Y652A cavity might still allow some current flow. Almost perpendicular positioning of the molecules is retrieved for the binding modes in the F656A mutant, but affinity of binding appears weaker than in the WT or Y652A cavities, rendering it an unstable plug against the K^+ current. Altogether, the physical obstruction coupled with the estimated binding affinity determines the block potency of the hERG channels by ligands.

4. Conclusion

Our dual-approach study strives to understand the molecular determinants underlying the stereoselectivity of hERG block by bupivacaine. Validation of our computational strategy using terfenadine, a chiral hERG blocker not reported to be stereoselective, was an important prerequisite of our work. Aromatic residues Tyr652 and Phe656, already known as crucial structural determinants for a majority of hERG blockers, were shown to be responsible for stereoselective differences in binding and block of this repolarizing K^+ channel. Polar residues located at the base of the selectivity filter, namely Ser624 and Thr623, also importantly contribute to bupivacaine recognition. The contribution of one additional α-subunit of the hERG channel for binding, together with the enhanced hydrogen-bonding network, is a central part of the molecular explanation for the higher current block experimentally observed for levo-(S)-bupivacaine. Molecular modeling results increased our understanding of the blocking effects of bupivacaine enantiomers on hERG WT channels. Similar *in silico* investigations were carried out with the hERG channel mutants Y652A and F656A. In both cases, binding modes and negligible differences in free

energy of binding between the bupivacaine enantiomers can explain the experimental results obtained with the patch clamp technique.

The final convergence of results, obtained from the computational investigation of enantiomeric block in an environment with rotational symmetry and the electrophysiological measurements of wild-type and mutated hERG channels, speaks in favor of the effectiveness of our target-based strategy. A more detailed understanding of the structural basis of binding could be acquired by studying structurally related molecules with experimental values of block. Jamieson et al. [42] reviewed the case of discrete structural modifications to design out hERG affinity in macrocyclic 3–aminopyrrolidinone farnesyltransferase inhibitors. Within this macrocyclic series, without changed in potencies of block of the pharmacological target, one (R,R)-compound presented high affinity towards hERG (IC_{50} = 0.15 μM), whereas its (S,R)–diastereoisomer did so to a lesser extent (~60-fold higher IC_{50}). A valuable medicinal chemistry strategy to contribute to the risk management of drug-induced LQTS would be to introduce chiral centers during lead optimization process followed by the evaluation of hERG-blocking properties of all enantiomers. In this perspective, the present work lays a robust foundation for a structure-based design approach to address hERG-related cardiotoxic problems currently faced during drug discovery and development.

5. Experimental section

5.1. Electrophysiology

5.1.1. Drugs

Racemic (R,S)-bupivacaine hydrochloride was obtained from Sigma–Aldrich and levo-(S)-bupivacaine hydrochloride was purchased from Brunschwig AG (Basel, Switzerland). Dextro-(R)-bupivacaine was kindly supplied by Cristália Ltd. (Itapira, SP, Brazil). Stock solutions (40 mM) were prepared in electrophysiological external solution ES5 (see *Patch clamp* section) and aliquots were kept at −20 °C. Final dilutions of bupivacaine were prepared daily.

5.1.2. Patch clamp

HEK293 cells were used 48 h after transient transfection with calcium phosphate technique using plasmid pcDNA3.1-(+)Zeo-hERG wild-type (WT), as previously described [14]. hERG mutants (gift from Dr. J. S. Mitcheson, University of Leicester, UK) were isolated from pSP64-hERG, subcloned into pcDNA3.1-(+)Zeo and the cDNA of final constructs was fully sequenced. Mutated hERG plasmids were transfected, similarly to WT plasmids, into HEK293 cells. Patch-clamp recordings in whole-cell configuration were carried out using an internal solution containing (mmol/L) KCl (145), EGTA (10), $MgCl_2$ (1), Mg-ATP (5) and HEPES (5), pH 7.30 with KOH. Three different K^+–concentration external solutions, or ES, were used according to the current amplitude on the hERG channels. All ES contained (mmol/L) $MgCl_2$ (1), $CaCl_2$ (2), D–Glucose (5) and HEPES (20), and pH 7.40 with NaOH. Differences between ES60, ES20 and ES5 were in K^+ and Na^+ concentrations, with KCl (60) and NaCl (85), KCl (20) and NaCl (125), and KCl (5) and NaCl (140), respectively. Measurements were carried out using an Axopatch 200B amplifier (Axon Instruments, Union City, CA), and were performed at room temperature (25 ± 1 °C) or 37 ± 1 °C, using a temperature control system TC2bip (Cell Micro Controls, Norfolk, VA) to heat the perfused solution. Constant flow (~250 μl/min) of perfusion was achieved with hydrostatic pressure. Voltage was stepped from a holding potential of −80 mV to +40 mV for 300 ms, followed by repolarization to −120 mV for 600 ms, applied at a frequency of 1.5Hz. To study current amplitude, peak tail currents were measured at −120 mV under perfusion of vehicle (I_{max}) followed by perfusion of enantiomer or racemic bupivacaine diluted in the same ES (I_{drug}) until steady-state was achieved. Inhibition was expressed as percent of inhibition compared to vehicle values of current (I_{max}/I_{drug}). Dose-response curves of inhibition were fitted by a Hill function described as:

$$y = \frac{100}{1 + 10^{(\log IC_{50} - x)}} \quad (1)$$

where y is the normalized current (% inhibition), x is the log of concentration, IC_{50} is the concentration producing half-maximal inhibition and k is the Hill slope.

Electrophysiological data are presented as mean ± standard error of the mean (SEM), and n indicates the number of cells treated per condition. Statistical significance ($P < 0.05$) was tested using a two-sided Student's t-test.

5.2. Molecular modeling

5.2.1. Selection and preparation of hERG target structures

Different publicly available homology models of the hERG channel were considered and meticulously evaluated as potential targets for the present computational studies. One of the published structures, based on the bacterial KvAP crystal (pdb entry:1orq), was provided by Farid et al. [31] and selected for two main reasons: i) the open conformation of the template channel appears suitable for drug binding and ii) it was built with the ligand (S)-terfenadine as an integral part of the structure using the so-called *induced-fit docking* protocol, which involves successive steps of Glide docking and Prime protein modeling [43]. Furthermore, this tridimensional structure was used by the authors as a docking target for binding mode prediction of well-characterized hERG blockers, including terfenadine, cisapride, sertindole, ibutilide and clofilium. The previous study yielded converging binding modes for all mentioned ligands, which added confidence to the poses obtained.

In the present study, i) all hydrogen atoms were added to the protein residues of the model by the procedure embedded in the BIOPOLYMER module of Sybyl 8.0 (Tripos Associates, Inc., St-Louis, MO), ii) (S)-terfenadine was removed, and iii) the remaining hERG structure was employed as input target (referred to as hERG WT) for docking simulations, without any further refinement or optimization.

For the generation of the mutant hERG structures (hERG Y652A and F656A), all four Tyr652 or Phe656 residues were mutated to alanine in the aforementioned hERG WT homology model using the BIOPOLYMER mutation tool provided within Sybyl 8.0. In order to correct for side chain reorganization at the vicinity of the manually-introduced mutation, hERG Y652A and F656A were subjected to slight conjugate gradient minimization by the Sander module of AMBER 10 [44] within the FF99SB force field, including implicit solvation according to the modified generalized Born model (GB/SA) developed by Onufriev et al. [45].

5.2.2. Preparation of terfenadine and bupivacaine ligand structures

Both enantiomers of terfenadine (i.e. 1-(4-*tert*-butylphenyl)-4-[4-[hydroxyl-di(phenyl)methyl]piperidin-1-yl]butan-1-ol) and both enantiomers of bupivacaine (i.e. 1–butyl-N-(2,6-dimethylphenyl)piperidine-2-carboxamide) were modeled with a protonated piperidine nitrogen, a formal charge of +1 and Gasteiger & Marsili partial atomic charges [46] within the Sybyl 8.0 environment. A first energy minimization was performed in the Tripos Force Field. Geometrical uncertainty about the piperidine rings stressed the need for deeper conformational searches using Spartan '06 (Wavefunction Inc, Irvine, CA). Cationic structures of terfenadine and bupivacaine were submitted to Monte Carlo (MC) analyses

according to the semi-empirical AM1 molecular orbital theory. Selected geometries were then optimized at HF/3-21G(*) level of theory. The lowest energy conformer of each compound was used as input ligand for GOLD docking towards hERG.

5.2.3. Automated flexible molecular docking

Molecular docking studies were carried out with the GOLD engine version 4.0 (CCDC Software Ltd., Cambridge, UK). The binding site was defined following the description of Stansfeld et al. [13], i.e. all protein atoms within 20 A from the natural K^+ ion S_{cav}. K^+ ions are not explicitly included in the hERG structure we used, therefore, coordinates were retrieved from the crystal subunit of KcsA including K^+ ions (pdb entry: 1k4c). The selectivity filter backbone was overlaid on our protein target and coordinates of potassium K3005 (corresponding to $S_{cav)}$ were set as the center of the binding site.

Three independent docking simulations, each calling for twenty solutions per ligand, were run in parallel according to the GOLD genetic algorithm default parameters. Ligands were considered as flexible and protein as rigid, except all hydroxyl and amine moieties. Moreover, on each subunit, the whole side chain of tyrosine at position 652, which is crucial for binding and can easily adapt its orientation, was considered as fully flexible according to the rotamer library available in GOLD 4.0. The dispersion of docking poses due to the rotational symmetry of the tetrameric target rendered examination and assessment of their goodness-of-fit difficult. For the sake of limiting this dispersing effect, a slight constraint favoring hydrogen-bonding with Ser624 of one specific subunit was applied, in accordance with the observations of Farid et al. [31].

The GoldScore fitness function with default parameters was employed for first evaluation and ranking of the sixty docking solutions returned for each ligand. Further criteria were applied to select one or a few more docking poses to be submitted to post-docking treatment: i) the population of clusters of solutions based on rmsd on heavy atoms, and ii) detailed visual inspection of intermolecular interactions involving *a priori* important pharmacophoric features, particularly the protonated nitrogen, the amide group and the aromatic rings.

5.2.4. Molecular mechanics post-docking optimization and binding affinity prediction

The estimated best virtual complexes, i.e. the selected docking solutions (according to the above-mentioned criteria) inside their corresponding hERG structure, were submitted to molecular mechanics treatment within the AMBER 10 environment. This post-docking procedure implied the traditional all-atom AMBER force field for the protein atoms, the GAFF force field and semi-empirical AM1–BCC charges for the ligand atoms, together with implicit solvation model terms. The protocol, adapted from Graves et al. [47], consists of three main steps where only the ligand is allowed to move inside the rigid protein channel: i) a 100-steps minimization with a conjugate gradient method, ii) a Langevin molecular dynamics of 3000 steps at constant temperature of 300K, and iii) a second minimization identical to i). The procedure, besides geometry optimization and refined binding mode prediction, leads to an approximation of ligand affinity for the hERG channel by estimating the free energy of binding (ΔG), according to the Equation (2):

$$\Delta G = E_{binding} = E_{complex} - \left(E_{protein} + E_{ligand}\right) \quad (2)$$

where $E_{complex}$, $E_{protein}$, E_{ligand} are the solvated internal energies of the complex, the protein and the ligand, respectively, as computed by the force fields enriched by implicit solvation terms according to the GB/SA model of Onufriev et al. [45] and the LCPO algorithm [48] term accounting for surface area.

5.2.5. Analysis of binding mode and intermolecular recognition

Geometries and intermolecular interactions within the optimized virtual complexes were visually analyzed using computer graphic facilities and with the help of Maestro 8.5 measurement tools (Schrödinger, LLC, Portland, OR). "Good contacts" were defined as atom radius ratio cutoff of 1.3 Å. Hydrogen-bond distance cut-off was set as 2.5 Å between both partner atoms; the minimum angles are set as 120° and 90 for donor and acceptor atoms, respectively.

A deeper exploration of the ligands' hydrogen-bonding properties was achieved by an in-house tool called Molecular Hydrogen-Bonding Potentials (MHBPs). MHBPs include two molecular interaction fields to model hydrogen-bonding donor ($MHBP_{do}$) and acceptor ($MHBP_{ac}$) capacities of conformations in the three-dimensional space. One of the advantages of this methodology is that it relies on an atomic fragmental system of donor (α) and acceptor (β) values, determined experimentally and not solely on geometrical considerations. It allows a precise and quantitative determination of the repartition of hydrogen-bonding properties around the molecule as measured in various solvents. Theoretical and technical details about MHBPs are given elsewhere [49,50]. For the specific purpose of assessing the balance between intramolecular and intermolecular hydrogen-bonding capacities of (R,S)-bupivacaine, $MHBP_{do}$ and $MHBP_{ac}$ were computed twice on a solvent accessible surface around the predicted binding conformations. Intramolecular forces were neglected during the first computation, but taken into account during the second.

Acknowledgements

The authors thank Dr. A. Nurisso and E. Favre (School of Pharmaceutical Sciences, Geneva, Switzerland) for their kind help and fruitful discussions regarding modeling, and M. Nenniger-Tosato (Department of Pharmacology and Toxicology, Lausanne, Switzerland) for the technical assistance in cell culture. We are also grateful to Dr. A. Felley Jacquemont for her thorough reading of the manuscript. We acknowledge Cristália Ltd. for generously supplying the pure (R)-enantiomer of bupivacaine and Dr. J. S. Mitcheson for the pSP64-hERG mutant constructs. The work was supported by grants of the Swiss National Science Foundation to H. Abriel (310030_120707). Part of this work was presented as a poster communication at the annual Fall Meeting of the Swiss Chemical Society (September 4th 2009, Lausanne, Switzerland). The poster was awarded a prize and the authors were invited to present their preliminary results in the special issue of the journal of the Swiss Chemical Society (Chimia) [51].

Appendix. Supplementary material

Supplementary data associated with this article can be found, in the online version, at doi:10.1016/j.ejmech.2011.05.015.

References

[1] M.C. Sanguinetti, C.G. Jiang, M.E. Curran, M.T. Keating, Cell 81 (1995) 299–307.
[2] M.E. Curran, I. Splawski, K.W. Timothy, G.M. Vincent, E.D. Green, M.T. Keating, Cell 80 (1995) 795–803.
[3] M.C. Sanguinetti, M. Tristani-Firouzi, Nature 440 (2006) 463–469.
[4] R. Dumaine, M.L. Roy, A.M. Brown, J. Pharmacol. Exp. Ther. 286 (1998) 727–735.
[5] D. Thomas, K. Wu, S. Kathöfer, H.A. Katus, W. Schoels, J. Kiehn, C.A. Karle, Brit. J. Pharmacol. 139 (2003) 567–574.
[6] S. Mohammad, Z.F. Zhou, Q.M. Gong, C.T. January, Am. J. Physio. Heart Circ. Physiol. 273 (1997) H2534–H2538.

[7] D.M. Roden, N. Engl. J. Med. 350 (2004) 1013–1022.
[8] R.R. Shah, Novartis. Found. Symp. 266 (2005) 251–280.
[9] E. Raschi, V. Vasina, E. Poluzzi, P.F. De, Pharmacol. Res. 57 (2008) 181–195.
[10] J.S. Mitcheson, J. Chen, M. Lin, C. Culberson, M.C. Sanguinetti, Proc. Natl. Acad. Sci. USA 97 (2000) 12329–12333.
[11] J.S. Mitcheson, Brit. J. Pharmacol. 139 (2003) 883–884.
[12] M.C. Sanguinetti, J.S. Mitcheson, Trends Pharmacol. Sci. 26 (2005) 119–124.
[13] P.J. Stansfeld, P. Gedeck, M. Gosling, B. Cox, J.S. Mitcheson, M.J. Sutcliffe, Proteins: Struct. Funct. Bioinf. 68 (2007) 568–580.
[14] C.B. Eap, S. Crettol, J.S. Rougier, J. Schläpfer, L. Sintra Grilo, J.J. Déglon, J. Besson, M. Croquette-Krokar, P.A. Carrupt, H. Abriel, Clin. Pharmacol. Ther. 81 (2007) 719–728.
[15] T. Gonzalez, C. Arias, R. Caballero, I. Moreno, E. Delpon, J. Tamargo, C. Valenzuela, Brit. J. Pharmacol. 137 (2002) 1269–1279.
[16] C.C. Siebrands, N. Schmitt, P. Friederich, Anesthesiology 103 (2005) 102–112.
[17] P. Friederich, A. Solth, S. Schillemeit, D. Isbrandt, Brit. J. Anaesth. 92 (2004) 93–101.
[18] S. Waldegger, G. Niemeyer, K. Mörike, C.A. Wagner, H. Suessbrich, A.E. Busch, F. Lang, M. Eichelbaum, Cell. Physiol. Biochem. 9 (1999) 81–89.
[19] K. Hartigan-Go, D.N. Bateman, A.K. Daly, S.H.L. Thomas, Clin. Pharmacol. Ther. (1996) 89–98.
[20] L. Sintra Grilo, P. Carrupt, H. Abriel, Front. Pharmacol. 1 (2010) 137.
[21] J.A. Sanchez-Chapula, T. Ferrer, R.A. Navarro-Polanco, M.C. Sanguinetti, Mol. Pharmacol. 63 (2003) 1051–1058.
[22] R.R. Shah, Br. J. Clin. Pharmacol. 54 (2002) 188–202.
[23] D. Rampe, M.L. Roy, A. Dennis, A.M. Brown, FEBS Lett. 417 (1997) 28–32.
[24] W.J. Crumb, J. Pharmacol, Exp. Ther. 292 (2000) 261–264.
[25] M.L. Roy, R. Dumaine, A.M. Brown, Circulation 94 (1996) 817–823.
[26] S.P. Pinney, B.S. Koller, M.R. Franz, R.L. Woosley, J. Cardiovasc, Pharmacol. 25 (1995) 30–34.
[27] C.C. Siebrands, P. Friederich, Anesthesiology 106 (2007) 523–531.
[28] J.T. Limberis, Z. Su, B.F. Cox, G.A. Gintant, R.L. Martin, Clin. Exp. Pharmacol. Physiol. 33 (2006) 1059–1065.
[29] M. Perry, P.J. Stansfeld, J. Leaney, C. Wood, M.J. de Groot, D. Leishman, M.J. Sutcliffe, J.S. Mitcheson, Mol. Pharmacol. 69 (2006) 509–519.
[30] R.M. Hardman, P.J. Stansfeld, S. Dalibalta, M.J. Sutcliffe, J.S. Mitcheson, J. Biol. Chem. 282 (2007) 31972–31981.
[31] R. Farid, T. Day, R.A. Friesner, R.A. Pearlstein, Bioorg. Med. Chem. 14 (2006) 3160–3173.
[32] J.T.K. Morgan, M.E. Sullivan, An overview of class III electrophysiological agents: a new generation of antiarrhythmic therapy. in: G.P. Ellis, D.K. Luscomb (Eds.), Prog. Med. Chem.. Elsevier Science Publishers, Amsterdam, 1992, pp. 65–108.
[33] R.A. Pearlstein, R.J. Vaz, J. Kang, X.L. Chen, M. Preobrazhenskaya, A.E. Shchekotikhin, A.M. Korolev, L.N. Lysenkova, O.V. Miroshnikova, J. Hendrix, D. Rampe, Bioorg. Med. Chem. Lett. 13 (2003) 1829–1835.
[34] A. Cavalli, E. Poluzzi, F. De Ponti, M. Recanatini, J. Med. Chem. 45 (2002) 3844–3853.
[35] H. Bardsley, R. Gristwood, H. Baker, N. Watson, W. Nimmo, Br. J. Clin. Pharmacol. 46 (1998) 245–249.
[36] K. Kamiya, R. Niwa, M. Morishima, H. Honjo, M.C. Sanguinetti, J. Pharmacol. Sci. 108 (2008) 301–307.
[37] R. Rajamani, B.A. Tounge, J. Li, C.H. Reynolds, Bioorg. Med. Chem. Lett. 15 (2005) 1737–1741.
[38] A.J. Labro, A.L. Raes, I. Bellens, N. Ottschytsch, D.J. Snyders, J. Biol. Chem. 278 (2003) 50724–50731.
[39] J.S. Mitcheson, J. Chen, M.C. Sanguinetti, J. Gen. Physiol. 115 (2000) 229–239.
[40] D. Fernandez, A. Ghanta, G.W. Kauffman, M.C. Sanguinetti, J. Biol. Chem. 279 (2004) 10120–10127.
[41] U. Zachariae, F. Giordanetto, A.G. Leach, J. Med. Chem. 52 (2009) 4266–4276.
[42] C. Jamieson, E.M. Moir, Z. Rankovic, G. Wishart, J. Med. Chem. 49 (2006) 5029–5046.
[43] W. Sherman, T. Day, M.P. Jacobson, R.A. Friesner, R. Farid, J. Med. Chem. 49 (2006) 534–553.
[44] D.A. Case, T.A. Darden, T.E. Cheatham, C.L. Simmerling, J. Wang, R.E. Duke, R. Luo, M. Crowley, R.C. Walker, W. Zhang, M. Merz, B. Wang, S. Hayik, G. Roitberg, G. Seabra, I. Kolossváry, K.F. Wong, F. Paesani, J. Vanicek, X. Wu, S.R. Brozell, T. Steinbrecher, H. Gohlke, L. Yang, C. Tan, J. Mongan, V. Hornak, G. Cui, D.H. Mathews, M.G. Seetin, C. Sagui, V. Babin, P.A. Kollman, AMBER 10. University of California, San Francisco, 2008.
[45] A. Onufriev, D. Bashford, D.A. Case, Proteins. Struct. Funct. Bioinf. 55 (2004) 383–394.
[46] J. Gasteiger, M. Marsili, Tetrahedron 36 (1980) 3219–3222.
[47] A.P. Graves, D.M. Shivakumar, S.E. Boyce, M.P. Jacobson, D.A. Case, B.K. Shoichet, J. Mol. Biol. 377 (2008) 914–934.
[48] J. Weiser, P.S. Shenkin, W.C. Still, J. Comput. Chem. 20 (1999) 217–230.
[49] S. Rey, G. Caron, G. Ermondi, P. Gaillard, A. Pagliara, P.A. Carrupt, B. Testa, J. Mol. Graphics Model. 19 (2001) 521–535.
[50] S. Rey, P.A. Carrupt, B. Testa, Ann. Pharm. Fr. 60 (2002) 386–396.
[51] L.S. Grilo, P.A. Carrupt, A. Daina, Chimia 64 (2010) 165–169.